

# Convective heat transport in stratified atmospheres at low and high Mach number

Evan H. Anders and Benjamin P. Brown

*Department of Astrophysical & Planetary Sciences, University of Colorado – Boulder and  
Laboratory for Atmospheric and Space Physics, Boulder, CO*

Convection in astrophysical systems is stratified and often occurs at high Rayleigh number (Ra) and low Mach number (Ma). Here we study stratified convection in the context of plane-parallel, polytropically stratified atmospheres. We hold the density stratification ( $n_\rho$ ) and Prandtl number (Pr) constant while varying the superadiabaticity and Ra. We find that Ma is primarily controlled by the superadiabaticity of the atmosphere. We also examine the behavior of the Nusselt number (Nu), which quantifies the efficiency of convective heat transport, and the Reynolds number (Re), which quantifies how turbulent our solutions are.

## INTRODUCTION

Convective heat transport is essential in the cores of high mass stars, the envelopes of low mass stars, and the atmospheres of terrestrial and jovian planets. These astrophysical systems have density stratifications ranging from a few density scale heights (e.g. massive star cores) up to 14 density scale heights in the convective envelopes of low mass stars such as the Sun. Atmospheric stratification presumably modifies the fundamental dynamics and heat transport mechanisms of these atmospheres. Understanding the fundamental properties of compressible convection in stratified media is essential to characterizing systems in astrophysics and planetary sciences. Numerical constraints have often restricted studies of compressible convection to moderately high Mach number (Ma), appropriate to regions near the Sun’s surface. Few fundamental properties of low Ma convection, which occurs in the deep solar interior, are known.

Early numerical experiments on stratified convection in two [1–4] and three [5, 6] dimensions revealed a number of basic properties in the moderate-to-high Ma regime. In the widely-studied Rayleigh-Bénard (hereafter RB) problem, upflows and downflows are symmetrical and the conductive flux approaches zero in the convective interior. These two hallmark characteristics of RB convection change significantly when stratification is included. Stratified convection exhibits narrow downflow lanes and broad upflow regions. Furthermore, the *entropy* gradient is negated by convection rather than the temperature gradient, and a significant conductive flux can exist in the presence of efficient convection.

In RB convection, there exist two primary control parameters: the Rayleigh number (Ra, the ratio of buoyant driving to diffusive damping) and the Prandtl number (Pr, the ratio of viscous to thermal diffusivity). These numbers coupled with the aspect ratio of the physical domain and the boundary conditions determine the dynamics of the convection. In stratified atmospheres, in addition to specifying the equation of state and fundamental properties of the gas, the two control parameters of RB convection are joined by the degree of stratifica-

tion across the domain and the characteristic Ma of the convective flows. Polytropically stratified atmospheres, such as those used in early studies [1–6], are an ideal extension of RB convection into the stratified realm because the two additional control parameters are directly linked to basic properties of the atmosphere. The density stratification is set by the number of density scale heights ( $n_\rho$ ) the atmosphere spans, and Ma is controlled by the superadiabatic excess ( $\epsilon$ ), the deviation of the polytropic index from the adiabatic polytropic index [1].

In this letter we study the behavior of convective heat transport, quantified by the Nusselt number (Nu), in plane-parallel, two-dimensional, polytropically stratified atmospheres. We vary  $\epsilon$  and Ra while holding  $n_\rho$ , Pr, and the aspect ratio constant. We describe experimental methods in section II, including the construction of atmospheres, equations, and numerical methods. Results are described in section III and their implications are discussed in section IV.

## EXPERIMENT

We examine the simplest stratified extension of RB by studying a fluid composed of monatomic ideal gas particles with an adiabatic index of  $\gamma = 5/3$  and whose equation of state is  $P = R\rho T$ . This is consistent with the approach used in earlier work. The initial atmosphere is a plane-parallel polytrope in which the gravitational acceleration and conductive flux,  $\mathbf{F}_{\text{cond},0} = -\kappa\partial_z T_0$ , do not vary with depth. To achieve the latter condition, both  $\kappa$  and  $\partial_z T_0$  are constant. Under these assumptions, satisfying hydrostatic equilibrium produces a stratification of

$$\begin{aligned}\rho_0(z) &= \rho_t(z_0 - z)^m, \\ T_0(z) &= T_t(z_0 - z),\end{aligned}\quad (1)$$

where  $m = m_{\text{ad}} - \epsilon$  is the polytropic index. The adiabatic polytropic index is  $m_{\text{ad}} \equiv (\gamma - 1)^{-1}$ , and the superadiabatic excess is  $\epsilon$  which sets the scale of the entropy gradient ( $\partial_z S_0 \propto -\epsilon$ ). A significant advance of this work is the ability to study large and small values of  $\epsilon$ , as will be discussed. Thermodynamic variables

are nondimensionalized at the top of the atmosphere as  $P_0(L_z) = \rho_0(L_z) = T_0(L_z) = 1$ , requiring  $z_0 \equiv L_z + 1$  and  $R = T_t = \rho_t = 1$ . By this choice, the non-dimensional length scale is the inverse temperature gradient scale and the timescale is the isothermal sound crossing time of this unit length. The height  $z$  increases upwards within  $[0, L_z]$ , where  $L_z = e^{n_\rho/m} - 1$  is determined by  $n_\rho$  and  $\epsilon$ . The characteristic timescale of convective dynamics is related to the atmospheric buoyancy time,  $t_b = \sqrt{L_z/g\epsilon}$ , with  $g = (m+1)$ . Throughout this letter, we use buoyancy time units and choose  $n_\rho = 3$  such that the initial density varies by a factor of 20. All atmospheres studied here have an aspect ratio of 4, such that  $L_x = 4L_z$ .

The atmospheric diffusivities are primarily controlled by the non-dimensional Rayleigh number,

$$\text{Ra} = \frac{gL_z^3(\Delta S_0/c_P)}{\nu\chi}, \quad (2)$$

where  $\Delta S_0 = \epsilon \ln z_0$  is the entropy difference between the top and bottom boundaries,  $c_P = R\gamma(\gamma-1)^{-1}$  is the specific heat at constant pressure,  $\nu$  is the kinematic viscosity (the viscous diffusivity), and  $\chi$  is the thermal diffusivity. The relationship between the thermal and viscous diffusivities is set by the Prandtl number,  $\text{Pr} = \nu/\chi$ . The dynamic viscosity,  $\mu$ , and the thermal conductivity,  $\kappa$ , relate to their corresponding diffusivities such that  $\nu \equiv \mu/\rho$  and  $\chi \equiv \kappa/\rho$ . We take  $\mu$  and  $\kappa$  to be constant with height. As a result,  $\text{Ra} \propto (\nu\chi)^{-1} \propto \rho^2$ . The atmospheres studied here with  $n_\rho = 3$  experience an increase in Ra by a factor of 400 across the domain. This formulation leaves  $\text{Pr}$  constant throughout the depth of the atmosphere. In this letter we impose  $\text{Pr} = 1$  and specify Ra at the top of the domain ( $z = L_z$ ).

While holding  $n_\rho$  and  $\text{Pr}$  constant, the primary control parameters of convection are  $\epsilon$  and Ra. We decompose our atmosphere into the background polytrope  $(\ln \rho_0, T_0)$  and the fluctuations about that background  $(\mathbf{u}, \ln \rho_1, T_1)$ , which can be large. The scaling of the entropy gradient with  $\epsilon$  is reflected in the evolved values of these fluctuations. For small  $\epsilon$ , evolved values scale as  $T_1/T_0 \propto \rho_1/\rho_0 \propto \text{Ma}^2 \propto \epsilon$ , as shown in Fig. 1.

We evolve the Fully Compressible Navier-Stokes equations,

$$\frac{\partial \ln \rho}{\partial t} + \nabla \cdot \mathbf{u} = -\mathbf{u} \cdot \nabla \ln \rho, \quad (3)$$

$$\frac{\partial \mathbf{u}}{\partial t} + \nabla T - \nu \nabla \cdot \bar{\boldsymbol{\sigma}} - \bar{\boldsymbol{\sigma}} \cdot \nabla \nu = -\mathbf{u} \cdot \nabla \mathbf{u} - T \nabla \ln \rho + \mathbf{g} + \nu \bar{\boldsymbol{\sigma}} \cdot \nabla \ln \rho, \quad (4)$$

$$\begin{aligned} \frac{\partial T}{\partial t} - \frac{1}{c_V} (\chi \nabla^2 T + \nabla T \cdot \nabla \chi) &= -\mathbf{u} \cdot \nabla T - (\gamma-1) T \nabla \cdot \mathbf{u} \\ &\quad + \frac{1}{c_V} (\chi \nabla T \cdot \nabla \ln \rho + \nu [\bar{\boldsymbol{\sigma}} \cdot \nabla] \cdot \mathbf{u}), \end{aligned} \quad (5)$$

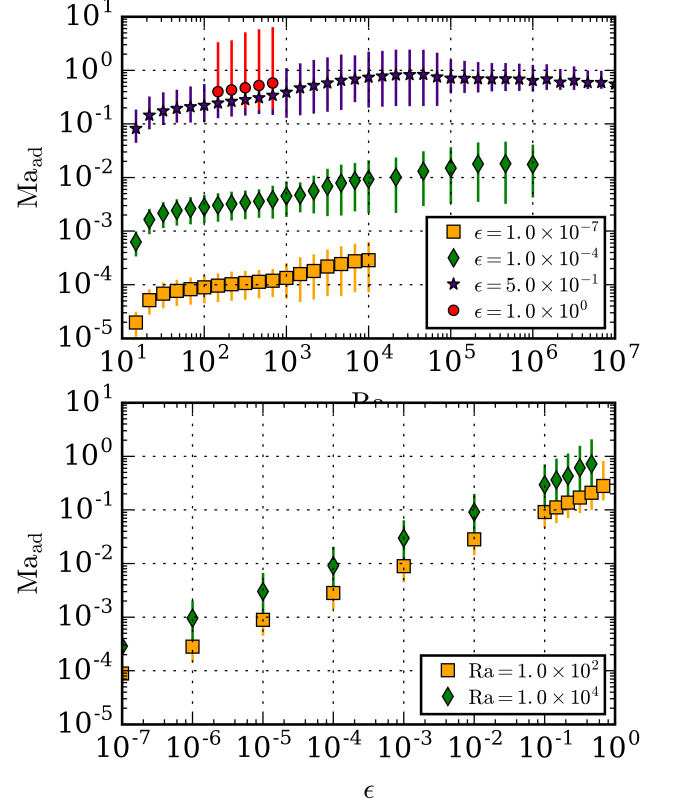


FIG. 1. The maximum value of Ma which has been horizontally averaged and time averaged for  $\geq 100t_b$ , beginning roughly  $50t_b$  after the start of simulations. This time average is long enough that the profile is well converged and error bars are negligible. (a) For  $\epsilon \leq 0.1$ , a scaling of  $\text{Ma} \propto \{\epsilon^{-0.50}, \epsilon^{-0.51}\}$  at  $\text{Ra} = \{10^2, 10^5\}$  exists. When  $\epsilon \rightarrow m_{\text{ad}}$ , large deviations from this power law are seen. (b) At high  $\epsilon$ , Ma scales as  $\text{Ra}^{0.28}$  until it reaches the supersonic regime, at which point it follows a power law of  $\text{Ra}^{-0.10}$ . At low  $\epsilon$ , consistent power laws are achieved throughout all values of Ra studied, where  $\text{Ma} \propto \{\text{Ra}^{0.26}, \text{Ra}^{0.22}\}$  for  $\epsilon = \{10^{-4}, 10^{-7}\}$ .

with the viscous stress tensor given by

$$\sigma_{ij} \equiv \left( \frac{\partial u_i}{\partial x_j} + \frac{\partial u_j}{\partial x_i} - \frac{2}{3} \delta_{ij} \nabla \cdot \mathbf{u} \right). \quad (6)$$

Taking an inner product of (4) with  $\mathbf{u}$  and adding it to (5) reveals the full energy equation,

$$\frac{\partial}{\partial t} \left( \rho \left[ \frac{|\mathbf{u}|^2}{2} + c_V T + \phi \right] \right) + \nabla \cdot (\mathbf{F}_{\text{conv}} + \mathbf{F}_{\text{cond}}) = 0, \quad (7)$$

where  $\mathbf{F}_{\text{conv}} \equiv \mathbf{F}_{\text{enth}} + \mathbf{F}_{\text{KE}} + \mathbf{F}_{\text{PE}} + \mathbf{F}_{\text{visc}}$  is the convective flux and  $\mathbf{F}_{\text{cond}} = -\kappa \nabla T$  is the conductive flux. The individual contributions to  $\mathbf{F}_{\text{conv}}$  are the enthalpy flux,  $\mathbf{F}_{\text{enth}} \equiv \rho \mathbf{u} (c_V T + P/\rho)$ ; the kinetic energy flux,  $\mathbf{F}_{\text{KE}} \equiv \rho |\mathbf{u}|^2 \mathbf{u}/2$ ; the potential energy flux,  $\mathbf{F}_{\text{PE}} \equiv \rho \mathbf{u} \phi$  (with  $\phi \equiv -gz$ ); and the viscous flux,  $\mathbf{F}_{\text{visc}} \equiv -\rho \nu \mathbf{u} \cdot \bar{\boldsymbol{\sigma}}$ , and each must be considered. Understanding how these

fluxes interact is crucial in characterizing convective heat transport.

The atmosphere is contained between two impenetrable, stress free, fixed temperature boundaries at the top and bottom of the domain such that  $w = \partial_z u = T_1 = 0$  at  $z = \{0, L_z\}$ . The domain is horizontally periodic. We utilize the Dedalus<sup>1</sup> [7] pseudospectral framework to time-evolve (3)-(5) using an implicit-explicit, third-order, four-step Runge-Kutta timestepping scheme RK443 [8]. Variables are time-evolved on a dealiased Chebyshev (vertical) and Fourier (horizontal) domain in which the physical grid dimensions are 3/2 the size of the coefficient grid. Physical grid sizes range from 96x384 grid points at the lowest values of Ra to 1152x4608 grid points at Ra  $\geq 10^7$ . By using IMEX timestepping, we implicitly step the stiff linear acoustic wave contribution and are able to efficiently study flows at moderate ( $\approx 1$ ) and very low ( $\approx 10^{-4}$ ) Ma (Fig. 1b). Our equations take the form of the FC equations in [9], extended to include variable  $\nu$  and  $\chi$ , and we follow the approach there; this IMEX approach has been successfully tested against a nonlinear benchmark of the compressible Kelvin-Helmholtz instability [10].

## RESULTS

The efficiency of convection is quantified by the Nusselt number. Nu is well-defined in RB convection as the total flux normalized by the steady-state conductive flux [11, 12]. In stratified convection Nu is more difficult to define, and we use a modified version of a traditional stratified Nusselt number [1, 3],

$$\text{Nu} \equiv \frac{\langle F_{\text{conv}, z} + F_{\text{cond}, z} - F_A \rangle}{\langle F_{\text{cond}, z} - F_A \rangle} = 1 + \frac{\langle F_{\text{conv}, z} \rangle}{\langle F_{\text{cond}, z} - F_A \rangle} \quad (8)$$

where  $F_{\text{conv}, z}$  and  $F_{\text{cond}, z}$  are the z-components of  $\mathbf{F}_{\text{conv}}$  and  $\mathbf{F}_{\text{cond}}$ , respectively and  $\langle \rangle$  implies a volume average.  $F_A \equiv -\langle \kappa \rangle \partial_z T_{\text{ad}}$  is the adiabatic conductive flux and  $\partial_z T_{\text{ad}} \equiv -g/c_P$  for an ideal gas in hydrostatic equilibrium. Here we specify  $\langle \kappa \rangle = \langle (\rho_1/\rho_0) \kappa_0 \rangle$ . At large values of  $\epsilon$ ,  $\kappa$  evolves significantly as the density profile evolves. At low  $\epsilon$ ,  $\langle \kappa \rangle \approx \kappa_0$ . In the Boussinesq approximation, under which  $\nabla S = 0$  only when  $\nabla T = 0$ , this definition reduces the the traditional definition of the Nusselt number [11, 12].

The Reynolds number and Peclet number,

$$\text{Re} = \frac{|u|L_z}{\nu}; \quad \text{Pe} = \text{Pr Re}, \quad (9)$$

quantify the importance of advection to diffusion in the evolved convective state. Our choice of  $\{\nu, \chi\} \propto \rho_0^{-1}$

drastically changes the value of Re between the top and bottom of the atmosphere. We report values of Re at the midplane ( $z = L_z/2$ ) of the atmosphere.

We evolve initial value problems in which  $T_1$  is filled with infinitesimal, random white noise compared to  $T_0$  and  $\epsilon$ . We filter the noise spectrum in coefficient space, such that 25% of the coefficients have power. Solutions were time-evolved until a long average of Nu showed little variance with depth. By performing a linear stability analysis, we determined that the onset of convection occurs at  $\text{Ra}_c = \{10.06, 10.97, 10.97\}$  for  $\epsilon = \{0.5, 10^{-4}, 10^{-7}\}$  respectively. We studied Rayleigh numbers from values at onset up to nearly  $10^6 \text{Ra}_c$  for  $\epsilon = \{0.5, 10^{-4}\}$  and up to  $10^3 \text{Ra}_c$  for  $\epsilon = 10^{-7}$ .

At large Ma ( $\epsilon = 0.5$ ), shock systems form in the upper atmosphere near downflow lanes (Fig. 2a) once Ra is sufficiently large. These shocks propagate through upflow regions. Such systems were reported in both two [4] and three [14] dimensional polytropic simulations previously. These shocks heat material entering the downflows, af-

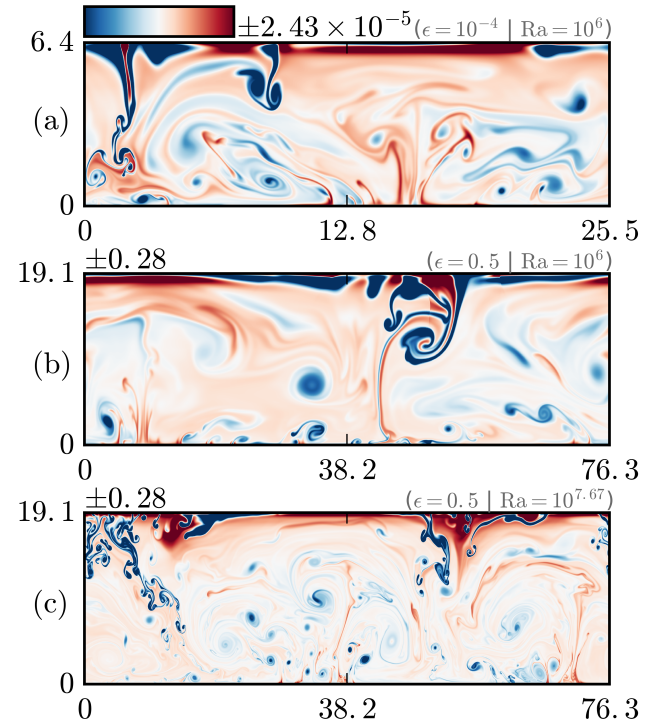


FIG. 2. Characteristic entropy fluctuations in evolved flows. The time- and horizontally-averaged profile is removed in all cases. (a) At high  $\epsilon$ , shock systems form near the upper downflow lanes ( $x \approx 45, z \approx 15-19$ ) at sufficiently high Ra. Shock-heated fluid then flows into the downflows as the shocks propagate across upflows. (b) At low  $\epsilon$  but at the same Ra, shock systems are absent, but otherwise the dynamics are similar. (c) As Ra is increased, downflows no longer span the entirety of the domain and individual small eddies are responsible for carrying the flux.

<sup>1</sup> <http://dedalus-project.org/>

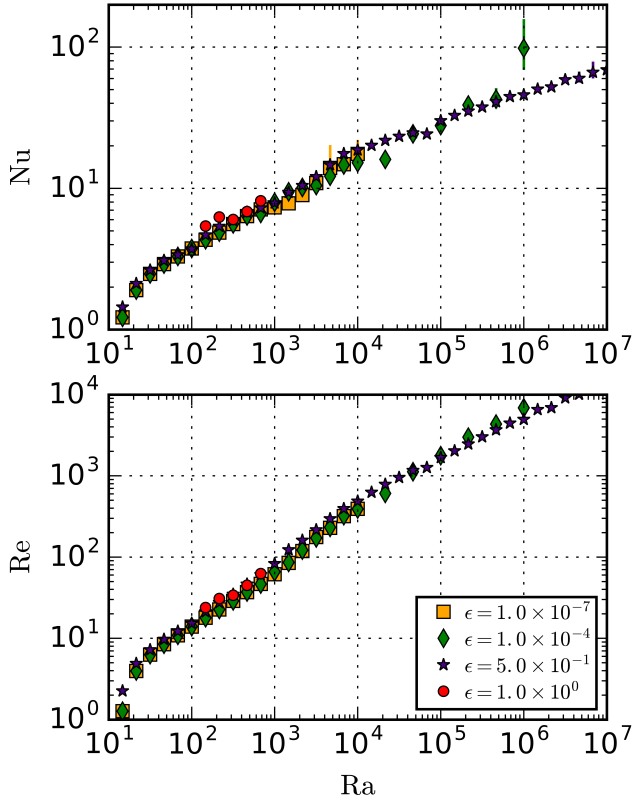


FIG. 3. Time-averaged vertical flux profiles ( $F_z$ ) for (a) high and (b) low Ma flows at  $\text{Ra} = 10^6$ . All fluxes are defined as in (7) and normalized by  $F_{\text{ref}} - F_A$ , as in (8). The dashed lines correspond to the enthalpy flux (orange, positive) and kinetic energy flux (purple, negative). The grey dash-dot line is the viscous flux and the green dotted line is the conductive flux with the adiabatic contribution removed. The potential energy flux is negligible and is not shown. In (a), the viscous flux is negligible and is not shown. The solid black line is  $\text{Nu}$ , the properly normalized sum of all the fluxes

fecting the dynamics and heat transport of these systems.

Low Ma flows ( $\epsilon = 10^{-4}$ ) have similar bulk thermodynamic structures (Fig. 2b) to high Ma flows. As  $\text{Ra}$  is increased to large values (Fig. 2c), thermodynamic structures no longer span the whole domain but rather break up into small eddies which traverse the domain multiple times before diffusing. While it has been suggested that pressure forces cause symmetry breaking in up- and downflows [3], at low  $\epsilon$  this effect seems to be secondary to flows obeying mass conservation as they traverse the stratified medium.

At large enough values of  $\text{Ra}$  for shocks to form, high Ma flows exhibit two local maxima in the enthalpy flux and kinetic energy flux (Fig. ??a). Shock-heated fluid parcels sometimes gain vorticity as they sink into the lower atmosphere. This creates deep, rapidly-rotating regions of mixing which persist for many overturn times. These “spinners” appear to influence the dynamics, but

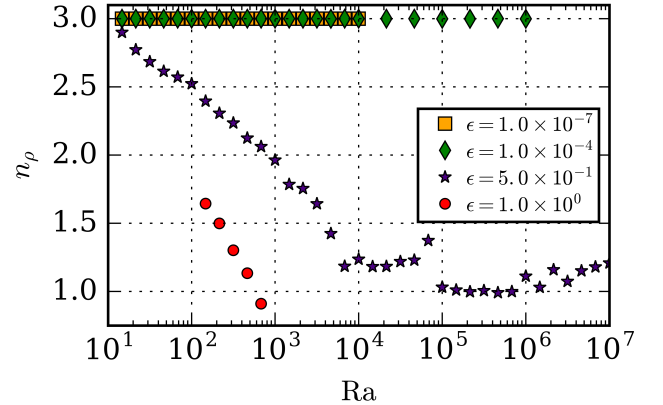


FIG. 4. Variation of  $\text{Nu}$  as  $\text{Ra}$  increases at high and low  $\epsilon$ . At high  $\epsilon$  (purple circles), a clear transition from the subsonic to supersonic regime is evident in the scaling of  $\text{Nu}$  with  $\text{Ra}$  at  $\text{Ra} \approx 10^4$ . In the low  $\epsilon$  regime (green diamonds and yellow squares), our observed  $\text{Nu}$  scalings collapse onto a similar line which is indistinguishable from a  $\text{Ra}^{2/7}$  scaling, as observed in RB convection [11]. Error bars are determined by the square root of the variance of the time-averaged  $\text{Nu}$  profile with depth and indicate whether or not a solution is well-converged.

their contributions are unclear.

At low Ma, only the deep maximum in enthalpy and kinetic energy fluxes is present (Fig. ??b). Our choice of fixed-temperature boundary conditions allows the flux at the boundaries to vary, so many runs at  $\text{Ra} > 10^5$  and  $\epsilon = 10^{-4}$  exhibit states in which the flux entering the system at the bottom of the atmosphere exceeds that which leaves at the top. These systems are punctuated by states of vigorous shearing, similar to those previously reported in two-dimensional RB convection [15]. During shearing states, convective transport is suppressed and  $\text{Nu}$  diminishes while excess energy exits the system through the upper boundary. A proper long-term average over shearing and non-shearing states retrieves an invariant  $\text{Nu}$  profile throughout the depth of the atmosphere. These shearing states will be covered in more detail in a future paper.

After appropriately time-averaging the fluxes for  $\geq 200t_b$ , a sensible flux average is retrieved. Nusselt numbers for all simulations at low and high Ma are plotted as a function of  $\text{Ra}$  in Fig. ???. At  $\epsilon = 0.5$ , in the near-sonic regime ( $\text{Ra} \leq 10^4$ ), the scaling of  $\text{Nu}$  with  $\text{Ra}$  is inflated, with  $\text{Nu} \propto \text{Ra}^{0.45}$ , similar to that expected in the ultimate regime of RB convection [16]. As simulations pass into the supersonic regime and shocks start to form near the downflows, that scaling drops to  $\text{Nu} \propto \text{Ra}^{0.19}$ . At  $\epsilon = \{10^{-4}, 10^{-7}\}$ , scaling laws of  $\text{Nu} \propto \text{Ra}^{\{0.31, 0.31\}}$  are retrieved. This scaling is indistinguishable from the  $\text{Ra}^{2/7}$  found in RB convection.

## DISCUSSION

In this letter we have studied fundamental heat transport by stratified convection in simplified 2-D polytropic atmospheres which are specified by two additional parameters,  $n_\rho$  and  $\epsilon$ . We argue that these atmospheres are the natural extension of the RB problem to stratified systems, and are an ideal laboratory for understanding the basic properties of stratified convection. The similarity between the scaling of Nu in RB convection and in our low- $\epsilon$  polytropes suggests that a boundary layer theory such as the Grossmann-Lohse theory for incompressible flows could be developed for fully compressible convection in these stratified systems [16].

The dynamics of these polytropic solutions are complex and time-dependent, even in two dimensions. Time-dependent oscillating shear states have developed spontaneously, as seen before in RB convection [15]. While computationally difficult, the highest values of Ra and the lowest value of  $\epsilon$  studied here are far from values found in nature. If the scalings of Nu and Ma presented here (Figs. 1 & ??) hold, then under solar conditions ( $\text{Ra} \approx 10^{20}$ ,  $\text{Ma} \approx 10^{-4}$ ), we expect that  $\epsilon \approx 10^{-20}$  and  $\text{Nu} \approx 10^6$ . Solar conditions are of course more complicated, as there  $\kappa$  is set by the radiative opacity, which depends on both  $\rho$  and  $T$ .

Future work will aim to better understand the mechanisms of shearing states and whether or not these states are attainable in three-dimensional, non-rotating atmospheres. Our studies here will serve as a foundation both for understanding and comparing heat transport in stratified convection to that in RB convection [11], and for future studies of transport in stratified convection in more realistic systems, such as rapidly rotating atmospheres [17], atmospheres bounded by stable regions [18], or regions with realistic profiles of  $\kappa$ .

### acknowledgements

EHA acknowledges the support of the University of Colorado's George Ellery Hale Graduate Student Fellowship. This work was additionally supported by NASA LWS grant number NNX16AC92G. Computations were

conducted with support by the NASA High End Computing (HEC) Program through the NASA Advanced Supercomputing (NAS) Division at Ames Research Center on Pleiades with allocations GID s1647 and GID g26133 (**AND ALSO THE NEW ONE AS OF 2017**). We thank Axel Brandenburg, Keith Julien, Mark Rast, and Jeff Oishi for many useful discussions.

- 
- [1] E. Graham, *Journal of Fluid Mechanics* **70**, 689 (1975).
  - [2] K. L. Chan, S. Sofia, and C. L. Wolff, *Astrophys. J.* **263**, 935 (1982).
  - [3] N. E. Hurlburt, J. Toomre, and J. M. Massaguer, *Astrophys. J.* **282**, 557 (1984).
  - [4] F. Cattaneo, N. E. Hurlburt, and J. Toomre, *ApJL* **349**, L63 (1990).
  - [5] F. Cattaneo, N. H. Brummell, J. Toomre, A. Malagoli, and N. E. Hurlburt, *Astrophys. J.* **370**, 282 (1991).
  - [6] N. H. Brummell, N. E. Hurlburt, and J. Toomre, *Astrophys. J.* **473**, 494 (1996).
  - [7] K. Burns, B. Brown, D. Lecoanet, J. Oishi, and G. Vasil, *Dedalus: Flexible framework for spectrally solving differential equations*, *Astrophysics Source Code Library* (2016), 1603.015.
  - [8] U. M. Ascher, S. J. Ruuth, and R. J. Spiteri, *Applied Numerical Mathematics* **25**, 151 (1997).
  - [9] D. Lecoanet, B. P. Brown, E. G. Zweibel, K. J. Burns, J. S. Oishi, and G. M. Vasil, *Ap. J.* **797**, 94 (2014), 1410.5424.
  - [10] D. Lecoanet, M. McCourt, E. Quataert, K. J. Burns, G. M. Vasil, J. S. Oishi, B. P. Brown, J. M. Stone, and R. M. O'Leary, *MNRAS* **455**, 4274 (2016), 1509.03630.
  - [11] H. Johnston and C. R. Doering, *Physical Review Letters* **102**, 064501 (2009), 0811.0401.
  - [12] J. Otero, R. W. Wittenberg, R. A. Worthing, and C. R. Doering, *Journal of Fluid Mechanics* **473**, 191 (2002).
  - [13] A. Brandenburg, K. L. Chan, Å. Nordlund, and R. F. Stein, *Astronomische Nachrichten* **326**, 681 (2005), astro-ph/0508404.
  - [14] A. Malagoli, F. Cattaneo, and N. H. Brummell, *ApJL* **361**, L33 (1990).
  - [15] D. Goluskin, H. Johnston, G. R. Flierl, and E. A. Spiegel, *Journal of Fluid Mechanics* **759**, 360 (2014).
  - [16] G. Ahlers, S. Grossmann, and D. Lohse, *Rev. Mod. Phys.* **81**, 503 (2009).
  - [17] K. Julien, E. Knobloch, A. M. Rubio, and G. M. Vasil, *Physical Review Letters* **109**, 254503 (2012).
  - [18] N. E. Hurlburt, J. Toomre, and J. M. Massaguer, *Astrophys. J.* **311**, 563 (1986).